

ON PRESSURIZED FUNCTIONALIZED PARTICLE-LADEN FLUID INFILTRATION INTO POROUS MEDIA

Tarek I. Zohdi¹ & Eduardo M.B. Campello^{2,*}

¹Department of Mechanical Engineering, University of California, 94720-1740, Berkeley, CA

²Department of Structural and Geotechnical Engineering, University of São Paulo, P.O. Box 61548, 05424-970, São Paulo, SP, Brazil

*Address all correspondence to: Eduardo M.B. Campello, Department of Structural and Geotechnical Engineering, University of São Paulo, P.O. Box 61548, 05424-970, São Paulo, SP, Brazil; Tel.: +55 11 3091-5489; Fax: +55 11 3091-5181, E-mail: campello@usp.br

Original Manuscript Submitted: 4/25/2018; Final Draft Received: 4/7/2019

In many emerging applications, the controlled infiltration of specially designed particle-laden fluids into porous media is critical. The added materials are often chosen with the objective to mechanically, electrically, or magnetically functionalize the overall material. Because of the increased viscosity of particle-laden fluids and the pore-dependent permeability of the medium to be infiltrated, there is a rich choice of parameters that govern the overall process: (i) the base viscosity of the solvent, (ii) the volume fraction of particles in the fluid, (iii) the pore volume fraction of the porous medium, and (iv) the absolute permeability of the medium. This paper develops Darcy-law-like expressions relating the infiltration flow rate of particle-laden fluids to the pressure gradient on porous solids, as a function of the four above parameters. General trends of the process may be satisfactorily described with the derived analytical expressions, yet at an affordable cost on accuracy for rapid daily design analysis. The paper then develops direct, large-scale numerical simulations based on the discrete element method to illustrate the practical use of the proposed relations.

KEY WORDS: *particle-laden fluids, infiltration, porous media, material functionalization, particles, discrete element method (DEM)*

1. INTRODUCTION

In a variety of industries, ranging from advanced manufacturing to translational medicine and geological exploration, the controlled infiltration of specially designed particle-laden fluids into porous media is of utmost importance. Often, the added materials are chosen with the objective to mechanically, electrically, or magnetically functionalize the overall material (see Fig. 1). Because of the increased viscosity of particle-laden fluids as compared to the raw (base) solvent and the pore-dependent permeability of the medium to be infiltrated, there is a rich choice of parameters that control the overall infiltration process:

- Base viscosity of the solvent
- Volume fraction of particles in the fluid
- Pore volume fraction of the porous medium
- Absolute permeability of the porous medium

Attempts to describe the flow of fluids through porous materials by means of simple analytical expressions date back to the experimental works of Darcy in the mid-nineteenth century. Since then, a variety of more refined

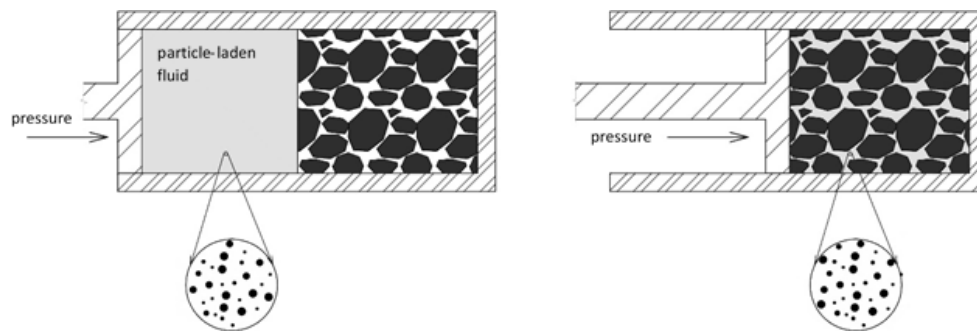


FIG. 1: Particle-laden fluid to be pumped into a porous solid (left) and the infiltrated solid (right)

models have been derived in the literature, especially boosted by the need to better understand the dynamics of aquifer, petroleum, and other reservoir formations. The contributions by Muskat and Meres (1936), Muskat (1937), and the many others that followed are especially noteworthy in this respect. From an engineering point of view, Darcy's law is very convenient due to its extreme simplicity. It provides reasonably accurate estimates to slow, viscous flow situations. It involves only very few parameters and physical properties of the flow, namely, the pressure drop experimented by the fluid in a given distance, the viscosity of the fluid, and the absolute permeability of the porous material. Yet, key macroscopic features are properly captured, such as: (i) no flow occurs in the absence of a pressure gradient within the porous medium; (ii) the flow occurs always from the higher to the lower pressure zones of the medium; (iii) the greater the pressure gradient in a given porous material is, the higher the fluid flow rate is; and (iv) for a given pressure gradient, the flow rate will always be different for different porous materials.

Darcy's law is only valid for single-phase, slow viscous flows—and in steady-state condition. Luckily, a great variety of natural and man-induced flows (e.g., groundwater flows and many industrial process flows) fall in this category. Indeed, any single-phase fluid flow with a Reynolds number less than 1–10 is typically laminar, and thereby may be satisfactorily described by Darcy's law. This paper explores the simplicity of Darcy's law and proposes Darcy-law-like expressions to describe the infiltration of two-phase (particle-laden) fluid flows through porous solids. We aim to relate the flow rate of such complex fluids to the pressure gradient observed within porous solids as a function of the four abovementioned control parameters. Our approach is based on the use of effective properties for both the two-phase fluid and the porous solid, as computed from rigorous bounds on effective responses for heterogeneous mixtures. The paper then focuses on a model problem and develops a computational framework based on the discrete element method (DEM) with which we perform direct numerical simulations to illustrate the practical use of the derived relations.

We remark that our objective in this work is to develop simple, semi-analytical expressions and a direct computational framework that can help guide analysts whose applications involve particle-laden fluid flows. Clearly, one could approach the problem with more elaborate analytical models, as well as with more complex, large-scale computational fluid dynamics (CFD) analyses. However, in the former case a larger number of model parameters would be required, some of which are not always readily available or straightforwardly obtainable in the laboratory. In the latter case, in turn, the numerical simulation of particle-laden continua with full fluid-particle interaction would require extremely fine spatiotemporal discretization grids, with several thousand numerical unknowns needed per particle length scale for numerically accurate results. For example, for several hundred thousand particles in a fluid (a typical situation), a proper discretization would imply several billion numerical unknowns, plus several million time steps for the simulation of even just a fraction of the flows' duration—a task that is certainly possible in high-performance computing centers, but obviously not practical for rapid daily design analysis. Here, instead, we aim to enable simple design and analysis tools with which analysts and engineers from industry may quickly assess the overall infiltration process, detecting general trends, identifying the relevance of certain parameters (and their subsequent impact on the flow), and rapidly drawing what-if scenarios. For examples on the full CFD approach, we refer the reader to Oñate et al. (2008, 2011, 2014), Rojek et al. (2012), Carbonell et al. (2010), Leonardi et al. (2014), Cante et al. (2014),

Bolintineanu et al. (2014), Avci and Wriggers (2012), and Zohdi (2007, 2014). This issue will be further discussed in Section 7.

The paper is organized as follows. In Section 2, we present our approach to deal with particle-laden fluids by means of effective properties. In Section 3, we do the same for dealing with heterogeneous porous materials. In Section 4, we derive our Darcy-like law. In Section 5, we introduce our DEM computational framework for simulation of such infiltration processes. In Section 6, we focus on a model problem and show examples of numerical simulations to illustrate the practical use of our scheme; whereas, in Section 7 we close the paper with some conclusions and final considerations. Throughout the paper, plain letters ($a, b, \dots, \alpha, \beta, \dots, A, B, \dots$) denote scalar quantities, whereas boldface italic letters ($\mathbf{a}, \mathbf{b}, \dots, \mathbf{A}, \mathbf{B}, \dots$) denote vectors in a three-dimensional Euclidean space. The (standard) inner product of two vectors is denoted by $\mathbf{u} \cdot \mathbf{v}$, and the norm of a vector by $\|\mathbf{u}\| = \sqrt{\mathbf{u} \cdot \mathbf{u}}$.

2. MODEL FOR EFFECTIVE PROPERTIES OF PARTICLE-LADEN FLUIDS

One simple approach to deal with complex, two-phase fluids is to work with an equivalent (homogenized) single-phase fluid, the properties of which being computed through rigorous bounds on effective responses for heterogeneous mixtures. In this sense, it is possible to characterize the effective properties of a particle-laden fluid as a function of the volume fraction of its particles and the properties of the baseline (solvent) fluid. The density of a particle-laden fluid is actually an effective density, since the fluid is, in reality, a mixture of particles and a solvent. Effective properties may be defined through volume averages. For example, the effective density ρ^* of the mixture (from now on, notation with a superscripted asterisk designates effective quantities) is

$$\rho^* = \langle \rho(\mathbf{x}) \rangle_V = \frac{1}{V} \int_V \rho(\mathbf{x}) dV = \frac{1}{V} \left(\int_{V_f} \rho_f dV + \int_{V_p} \rho_p dV \right) = v_f \rho_f + v_p \rho_p \tag{1}$$

where $\rho(\mathbf{x})$ is the density of the material point located at position \mathbf{x} , V is the volume of the mixture, ρ_f and ρ_p are the densities of the baseline fluid and the particles, respectively, and v_f and v_p are the volume fractions of the fluid and particles, respectively. The volume fractions have to sum to unity

$$v_f + v_p = 1 \Rightarrow v_f = 1 - v_p \tag{2}$$

Similar approaches can be used to calculate various types of properties, such as the fluid’s effective viscosity—a transport property. However, these calculations are a bit more complicated, because they require one to estimate the types of interactions between the constituents. There are a number of models that provide expressions for the effective viscosity of a fluid containing particles. For example, if one considers that the particles are rigid relative to the surrounding fluid (a valid assumption for the purposes of this work), one possible expression is as proposed by Einstein (1906) in the early 1900s

$$\mu^* = \mu_f (1 + 2.5v_p) \tag{3}$$

where μ_f is the viscosity of the baseline (incompressible) fluid. This approximation is quite simple but only valid at extremely low volume fractions of particles ($< 1\%$). At quite moderate to high volume fractions, it is very inaccurate. A better approximation, which is in fact a rigorous lower bound on the effective viscosity, can be derived by resorting to Hashin-Shtrikman bounds (Hashin and Shtrikman, 1962, 1963; Hashin, 1983) on effective responses for two-phase solid mixtures. Accordingly, for linear elasticity (solid mechanics) applications, for a mixture of two isotropic materials, each with bulk modulus κ_1 and κ_2 , shear modulus G_1 and G_2 , and volume fractions v_1 and v_2 , the bounds for the effective bulk modulus are

$$\begin{aligned} \kappa_1 + \frac{v_2}{[1/(\kappa_2 - \kappa_1)] + [3(1 - v_2)/(3\kappa_1 + 4G_1)]} &\leq \kappa^* \leq \kappa_2 \\ + \frac{1 - v_2}{[1/(\kappa_1 - \kappa_2)] + [3v_2/(3\kappa_2 + 4G_2)]} & \end{aligned} \tag{4}$$

whereas, for the effective shear modulus, they are

$$G_1 + \frac{v_2}{[1/(G_2 - G_1)] + \{[6(1 - v_2)(\kappa_1 + 2G_1)]/[5G_1(3\kappa_1 + 4G_1)]\}} \leq G^* \leq G_2$$

$$+ \frac{1 - v_2}{[1/(G_1 - G_2)] + \{[6v_2(\kappa_2 + 2G_2)]/[5G_2(3\kappa_2 + 4G_2)]\}}$$
(5)

wherein it is implicitly assumed that $\kappa_2 \geq \kappa_1$ and $G_2 \geq G_1$. In this case, phase 1 is the softer (usually matrix) material; whereas, phase 2 is the stiffer (usually particulate) one. To adapt these expressions to a mixture comprised of rigid particles and a matrix fluid, we first take the limit of the particle phase becoming infinitely rigid as compared to the fluid phase (i.e., $\kappa_2 \rightarrow \infty$ and $G_2 \rightarrow \infty$, with the elastic shear modulus G_1 playing the role of the fluid viscosity μ_f). Then, we assume that the fluid is incompressible (i.e., $\kappa_1/G_1 \rightarrow \infty$), such that from the lower bound of Eq. (5) (and after some algebra), we arrive at

$$\mu^{*, -} = \mu_f \left(1 + 2.5 \frac{v_p}{1 - v_p} \right)$$
(6)

wherein notation with a superscripted minus sign is introduced to designate lower bounds. This expression is the tightest known lower bound on the effective viscosity of a two-phase material comprised of rigid particles in a surrounding incompressible fluid, provided that the volume fractions and constituent viscosities are the only known information about the microstructure of the mixture. It is valid for isotropic phases with isotropic effective responses and remains quite accurate up to about $v_p = 0.15$, which is sufficient for most applications in which we are interested in this work. Note that no geometric or direct statistical information is required for such a bound. Also, note that it recovers Einstein's result in the zero particle volume fraction limit ($v_p \rightarrow 0$), while still providing a rigorous estimate at quite significant values of v_p (as said, up to 15%). The lower bound is a good approximation to the effective viscosity of a mixture whenever the mixture is composed of highly stiff particles surrounded by a low stiffness matrix, which is precisely the case here. Thereby, in all applications we deal with in this work, we set $\mu^* = \mu^{*, -}$.

As will be shown in Section 4, expression (6) allows us to directly correlate the pressure gradient in a heterogeneous porous material to the volume fraction of particles in a particle-laden fluid. For an authoritative review of the general theory of random heterogeneous media, we refer the reader to (Torquato, 2002). For more mathematical homogenization aspects, see, e.g., Jikov et al. (1994); whereas, for solid mechanics inclined accounts of the subject (besides the already mentioned works by Hashin and Shtrikman, see Mura (1993) and Markov (2000).

3. MODEL FOR EFFECTIVE PERMEABILITY OF HETEROGENEOUS POROUS MEDIA

In a similar way as in Section 2, one simple approach to deal with complex (inherently heterogeneous) porous solid media is to work with an equivalent (homogenized) single-phase solid, the properties of which being computed through bounds on effective responses for heterogeneous solid mixtures. Accordingly, it is possible to estimate the effective permeability of a porous material (prior to its infiltration by a fluid) as a function of the volume fraction of its constituents and their individual permeabilities (assuming that both phases are isotropic). These estimates provide one with upper and lower bounds on the overall response of the material. The underlying steady conservation law is

$$\nabla \cdot \mathbf{G} = \nabla \cdot (-P^* \nabla p) = 0$$
(7)

where

$$\mathbf{G} = -P^* \nabla p$$
(8)

is the flux of energy (N · m) per unit area, P^* is the effective permeability of the medium (with units of m^2), and ∇p is the pressure gradient within the overall material. For two isotropic solid phases, each with known permeability P_1 and P_2 (pre-infiltration) and volume fractions v_1 and v_2 , the following estimates may be derived from Hashin-Shtrikman bounds:

$$P_1 + \frac{v_2}{[1/(P_2 - P_1)] + [(1 - v_2)/3P_1]} \leq P^* \leq P_2$$

$$+ \frac{1 - v_2}{[1/(P_1 - P_2)] + (v_2/3P_2)}$$
(9)

where

$$P^{*,-} = P_1 + \frac{v_2}{[1/(P_2 - P_1)] + [(1 - v_2)/3P_1]}$$

and

$$P^{*,+} = P_2 + \frac{1 - v_2}{[1/(P_1 - P_2)] + (v_2/3P_2)} \quad (10)$$

are the lower and upper bounds, respectively. Here, it is implicitly assumed that $P_2 \geq P_1$, i.e., phase 2 is the more “conductive” or permeable material; whereas, phase 1 is the less permeable one. Typically, two cases of material combinations may be considered in such mixtures: one comprised of a tight, less permeable solid matrix that surrounds softer, highly permeable particles (denoted case 1), and the other comprised of a softer, highly permeable matrix surrounding denser, stiff (less permeable) particles (denoted case 2). Case 1 may correspond, e.g., to a spongelike material, with the particles representing the pores; whereas, case 2 may correspond to, e.g., a granular material, with the particles standing for the grains. As before, provided that the volume fractions and constituent permeabilities are the only known information about the microstructure of the medium (prior to its infiltration), the expressions above are the tightest bounds for the overall isotropic effective (pre-infiltration) permeability of two-phase media, where both constituents are isotropic. A critical observation is that the lower bound is more accurate for materials that resemble case 1 at low particle volume fractions, and even more so if the particles are nearly spherical, such that they make little or no contact with each other. In these cases, the matrix will isolate the highly permeable zones and the overall system will be less permeable. The upper bound, in turn, is more accurate for materials that resemble case 2 at low to moderate particle volume fractions, wherein the permeable matrix prevails.

The typical use of the bounds given by Eqs. (9) and (10) is to form a convex combination as follows:

$$P^* \approx (1 - \varphi^{perm})P^{*,-} + \varphi^{perm}P^{*,+} \quad (11)$$

where $\varphi^{perm} \in [0,1]$ is a scalar parameter such that:

- if $\varphi^{perm} = 0$, we have the lower bound
- if $\varphi^{perm} = 1$, we have the upper bound
- if $\varphi^{perm} = 1/2$, we have the average of the bounds.

Ultimately, φ^{perm} is a function of the microstructure of the medium prior to its infiltration and must be calibrated. This can be done from known qualitative information on its microstructural features. For example, for case 1 materials at low particle volume fractions (for example, under 15%), with spherical particles that are not making contact, the lower bound is more accurate, as mentioned, and thus one would pick $\varphi^{perm} = \varphi^{perm,sph} < 0.5$ to bias the estimate to the lower bound. If, however, we take the same volume fraction but make the particles long flat flakes instead of spheres (but yet randomly oriented, such that no preferred direction builds up and the isotropy assumption is not violated), they will certainly touch, thereby producing highly permeable pathways that will increase the system’s overall permeability, and thus one would pick $\varphi^{perm} = \varphi^{perm,fl} > \varphi^{perm,sph} <$.

One can calibrate φ^{perm} by comparing it to different experiments. This was done before, for example for mechanical properties, in Zohdi et al. (2002). Essentially, for case 1 materials, the more the material of phase 2 interacts, for example physically touching, the more the upper bound becomes relevant, and vice-versa. Similar considerations may be derived for case 2 materials. The general trends are: (a) for cases where the upper bound is more accurate, such as $\varphi^{perm} > 0.5$ and (b) for cases where the lower bound is more accurate, such as $\varphi^{perm} < 0.5$. In an overall sense, provided that isotropy holds for the individual solid phases and for the effective response, φ^{perm} indicates the degree of interaction between the mixture’s constituents.

4. INFILTRATION OF PARTICLE-LADEN FLUIDS IN HETEROGENEOUS POROUS MEDIA: A DARCY-LIKE LAW

A Darcy-like law to describe the infiltration of multiphase fluids into heterogeneous porous solids is one that postulates simple proportional relationships between the volumetric flow rate Q (measured in cubic meters per second), the effective viscosity of the fluid (μ^*) and the pressure drop over a given distance L within the solid

$$Q = -\frac{P^*A(p^+ - p^-)}{\mu^*L} \quad (12)$$

where P^* is the effective permeability of the solid medium, A is the cross-sectional area to the flow, and $(p^+ - p^-)$ is the total pressure drop experienced by the fluid over L (p^+ is the fluid pressure at the inlet and p^- at the outlet of the flow). Dividing the above expression by A yields

$$q = -\frac{P^*}{\mu^*}\nabla p \quad (13)$$

where $q = Q/A$ is the so-called Darcy flux (i.e., volumetric flow rate per unit area, measured in meters per second), and

$$\nabla p = \frac{p^+ - p^-}{L} \quad (14)$$

is the pressure gradient. By combining the expressions of the effective viscosity and effective permeability derived in Sections 2 and 3 (i.e., by assuming that the multiphase fluid is comprised of rigid particles at low to moderate volume fractions in a surrounding incompressible fluid matrix, and that the porous solid medium is consisted of two phases with known individual permeabilities), we obtain the following:

$$q = -\frac{P^*}{\mu^*}\nabla p \approx -\frac{\varphi^{perm}P^{*,-} + (1 - \varphi^{perm})P^{*,+}}{\mu^{*,-}}\nabla p \quad (15)$$

or more explicitly, with the aid of Eqs. (6) and (10)

$$q \approx -\frac{\varphi^{perm} \left(P_1 + \frac{v_2}{[1/(P_2 - P_1)] + [(1 - v_2)/3P_1]} \right) + (1 - \varphi^{perm}) \left(P_2 + \frac{1 - v_2}{[1/(P_1 - P_2)] + (v_2/3P_2)} \right)}{\mu_f (1 + 2.5[v_p/(1 - v_p)])} \nabla p \quad (16)$$

From Eq. (16), an analytical relation for the pressure-gradient-to-flow-rate ratio ($\nabla p/q$) follows, which is a very useful measure to describe the overall infiltration process. It allows one to estimate what pressure gradient is needed to maintain a desired flow rate during a (slow, Darcy-like) particle-laden fluid infiltration, or conversely, what is the flow rate that follows from a given pressure gradient within a heterogeneous porous material in such types of flow. Note that this ratio is a function of the four control parameters mentioned in Section 1: the base viscosity of the solvent, the volume fraction of the particles, the pore volume fraction of the porous solid, and the permeability of the solid's constituents. Note also that the only difference between the classical (single-phase flow) Darcy's law and the one proposed here is the enabling of multiphase fluids through the use of effective properties. In addition, a rational procedure is proposed to estimate the permeability of the heterogeneous porous material based solely on the known permeability of its constituents and their corresponding volume fractions. These features allow us to arrive at a very simple and convenient expression for the pressure-gradient-to-flow-rate ratio, as follows from Eq. (16).

5. DEM FRAMEWORK FOR SIMULATION OF PARTICLE-LADEN FLUID INFILTRATION

For rapid simulation of particle-laden fluids infiltrating porous solid media, our computational framework is based on a direct, purely DEM model to represent both the particles of the fluid and the solid phase of the porous material. No continuum phase is involved. The presence of the fluid is only indirectly considered, through drag and pressure forces acting on the particles. We follow the DEM formulation derived by Zohdi (2012), Campello (2015a,b, 2018),

and Campello and Zohdi (2014a,b), but we will not report it in detail here for the sake of brevity. In general lines, it consists of a soft-sphere model (i.e., one in which the particles' contacts are described by means of forces given as a function of the local deformations at the contact points, through some constitutive equation), wherein drag forces, pressure forces, near-field forces, contact forces (through Hertz contact theory), friction forces (with stick-slip phenomena), and rolling resistance effects are all taken into account within an updated Lagrangian description of the particles' motion. Solution of the system's dynamics is pursued through implicit (or occasionally explicit) time integration of the equations of motion, coupled with a recursive (fixed-point iteration) scheme for resolving the complex multiparticle interactions. Note that the model considers only a one-way type of "coupling" between the particles and the fluid, in the sense that, the particles are affected by the fluid but the fluid is not affected (or at most is only negligibly affected) by the particles, and thereby not resolved.

The drag forces from the fluid on the particles are computed by means of the classical drag equation [see, e.g., Biringen and Chow (2011)], coupled with a Reynolds-dependent drag coefficient as follows:

$$\mathbf{f}_i^{drag} = -\frac{1}{2}\rho_f C_D A_i \|\mathbf{v}_i - \mathbf{v}_f\| (\mathbf{v}_i - \mathbf{v}_f) \quad (17)$$

where ρ_f is the mass-density of the fluid, C_D is the drag coefficient, $A_i = \pi r_i^2$ is the "frontal" area of particle i (of radius r_i) with respect to the flow, \mathbf{v}_i is the particle's velocity, and \mathbf{v}_f is the velocity of the fluid at the particle's location. The drag coefficient is given according to the model by Biringen and Chow (2011) for smooth spheres

$$\begin{aligned} \text{for } 0 < \text{Re} \leq 1, & \quad C_D = 24\text{Re}^{-1} \\ \text{for } 1 < \text{Re} \leq 400, & \quad C_D = 24\text{Re}^{-0.646} \\ \text{for } 400 < \text{Re} \leq 3 \times 10^5, & \quad C_D = 0.5 \\ \text{for } 3 \times 10^5 < \text{Re} \leq 2 \times 10^6, & \quad C_D = 0.000366\text{Re}^{0.4275} \\ \text{for } \text{Re} > 2 \times 10^6, & \quad C_D = 0.18 \end{aligned} \quad (18)$$

where

$$\text{Re} = \frac{2\rho_f r_i \|\mathbf{v}_i - \mathbf{v}_f\|}{\mu_f} \quad (19)$$

is the Reynolds number at the particle's location, with μ_f as the fluid's viscosity. The assumption that C_D is dependent on Re is valid for incompressible flows, which is the case here. The fluid's velocity field, \mathbf{v}_f , is assumed to be known (given).

The pressure forces, in turn, are computed as the net force that results from the pressure difference at the front and back faces of a particle with respect to the direction of the flow, i.e.

$$\mathbf{f}_i^{press} = -[p(\mathbf{x}_i + \Delta\mathbf{x}) - p(\mathbf{x}_i - \Delta\mathbf{x})]A_i \mathbf{n}_f = -2r_i \nabla p A_i \mathbf{n}_f \quad (20)$$

where $p(\mathbf{x}_i + \Delta\mathbf{x})$ and $p(\mathbf{x}_i - \Delta\mathbf{x})$ are the pressures of the fluid at the particle's front and back faces relative to the flow, respectively, \mathbf{x}_i is the position vector of the particle, $\Delta\mathbf{x}$ is the vector distance from the particle's center to the particle's surface in the direction of the flow, and \mathbf{n}_f is the unit vector that gives the direction of the flow (or, equivalently, the direction of the pressure gradient). Note that, consistent with Darcy's assumption, it is implicitly considered that the pressure gradient is constant in the direction of the flow. Also, body forces from the fluid are neglected.

For a thorough description of the other forces (contact, friction, and occasionally near-field forces), as well as moments with respect to the centers of the particles, we refer the reader to Zohi (2012) and Campello (2015a, 2018). These forces and moments enter Euler's laws for every particle of the system, which are then solved via numerical time integration combined with a recursive (fixed point iteration) scheme for solution of the multiparticle interactions. Such integration has to be performed with appropriate time-step sizes. For sufficiently accurate results, one criterion that must be fulfilled is

$$\Delta t \leq \frac{\delta t_{con}}{10}, \quad \delta t_{con} \cong 2.87 \left[\frac{(m^*)^2}{r^*(E^*)^2 v_{rel}} \right]^{1/5} \quad (21)$$

where δt_{con} is the duration of the fastest contact among all particle contacts of the system, with v_{rel} as the relative velocity of the corresponding contacting pair in the pair's central direction immediately before the contact is initiated, and m^* , r^* , and E^* as the effective mass, effective radius, and effective elasticity modulus of the pair. This is based on Hertz's contact theory [see Johnson (1985)] and, according to our experience, allows for a good accuracy in the integration of the contact forces, which are the critical forces in the model.

6. EXAMPLE

To illustrate how the analytical expressions and computational framework presented above may be used to perform practical calculations on infiltration processes, let us consider a model problem consisting of the pressurized infiltration of a granular solid. The solid is comprised of dense particles of very low permeability (forming the less permeable zones) embedded in a matrix of a continuous, ultralight material of much higher permeability (forming the highly permeable zones), similar to what is depicted in Fig. 1. We take the following properties for the particle-laden fluid and the granular solid:

- Mass density of the base fluid solvent, $\rho_f = 2 \times 10^3 \text{ kg/m}^3$
- Mass density of the particles carried in the fluid, $\rho_p = 7 \times 10^3 \text{ kg/m}^3$
- Mass density of the less permeable zones of the granular solid (pre-infiltration), $\rho_1 = 5 \times 10^3 \text{ kg/m}^3$
- Mass density of the highly permeable zones of the granular solid (pre-infiltration), $\rho_2 = 0$
- Viscosity of the base fluid solvent, $\mu = 0.001 \text{ Pa} \cdot \text{s}$
- Volume fraction of the particles carried in the fluid, $v_p = 0.15$
- Volume fraction of the less permeable zones of the granular solid, $v_1 = 0.55$
- Volume fraction of the highly permeable zones of the granular solid, $v_2 = 1 - v_1 = 0.45$
- Permeability of the less permeable zones of the granular solid (pre-infiltration), $P_1 = 10^{-9} \text{ m}^2$
- Permeability of the highly permeable zones of the granular solid, $P_1 = 10^{-6} \text{ m}^2$

By using the expressions presented in Sections 2–4 and setting $\varphi^{perm} = 0.5$, we arrive at the following set of effective properties:

- Effective mass density of the particle-fluid mixture: $\rho^* = 2750 \text{ kg/m}^3$
- Effective viscosity of the particle-fluid mixture: $\mu^* = 0.00144 \text{ Pa} \cdot \text{s}$
- Effective permeability of the granular solid (prior to infiltration): $P^* = 1.84 \times 10^{-7} \text{ m}^2$
- Pressure-gradient to flow-rate ratio: $\Delta p/q = -7.82 \times 10^3 \text{ Pa} \cdot \text{s/m}^2$

Let us now consider that the lengths of the model, those indicated in Fig. 2. The particles carried by the fluid have radii following a Gaussian distribution of mean $\bar{r} = 0.0015 \text{ m}$ and standard deviation $\sigma_r = 0.0001 \text{ m}$, truncated at three standard deviations from the mean such that all radii fall in the interval $r_i \in [0.0012 \text{ m}, 0.0018 \text{ m}]$. Their elastic properties are elasticity modulus $E_i = 10^7 \text{ N/m}^2$ and Poisson coefficient $\nu_i = 0.25$. For the granular solid, in turn, we consider a cubic specimen with exterior dimensions $0.1 \times 0.1 \times 0.1 \text{ m}$ (see Fig. 2), within which the particles (i.e., grains) are randomly distributed in a nonoverlapping way at the volume fraction of $v_1 = 0.55$, as listed above. The radii of the grains follow a Gaussian distribution of mean $\bar{r} = 0.01 \text{ m}$ and standard deviation $\sigma_r = 0.001 \text{ m}$, also truncated at three standard deviations from the mean, such that all radii fall in the interval $r_i \in [0.007 \text{ m}, 0.013 \text{ m}]$. The grains are assumed to be immovable within the specimen, as if the granular solid had an infinitely rigid fabric

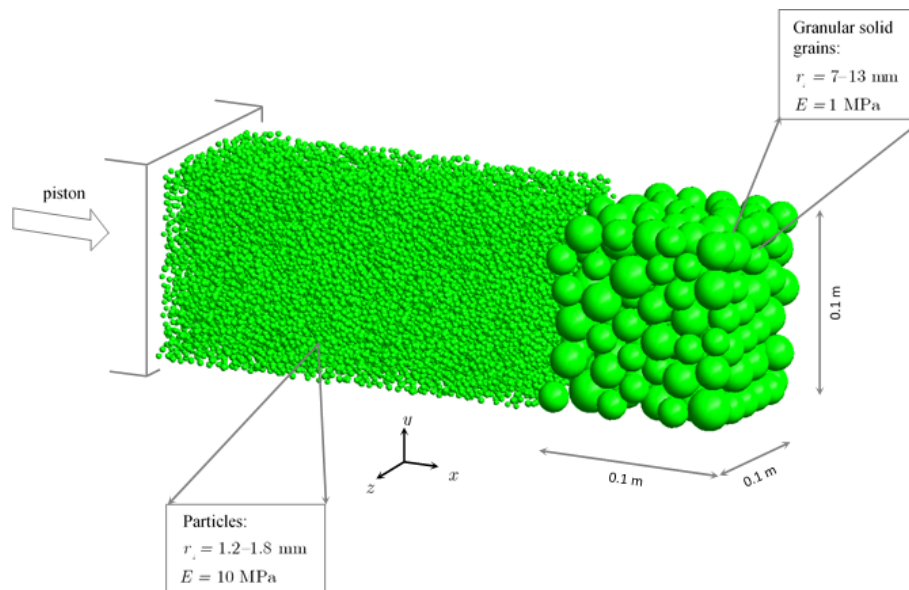


FIG. 2: Model problem: pressurized infiltration of a granular solid (schematic illustration)

structure. Their elastic properties are $E_i = 10^6$ N/m² and $\nu_i = 0.25$. For both the fluid and granular solid, the particles are generated using a random-sequence addition scheme that fully complies with the given radius' Gaussian distributions [see, e.g., Campello and Cassares, (2016)]. With the system at rest, the infiltration is initiated by a pressurized piston that drives both the fluid and particles toward the granular solid with a constant acceleration of $a = 2.143$ mm/s² (this is the same acceleration that the particles would experience if a pressure gradient of 0.01 kPa/m existed before the specimen). Inside the specimen, in turn, a pressure gradient of ∇p in the direction $\mathbf{n}_f = (1, 0, 0)$, with various intensities, is applied. The specimen is entirely enclosed by lateral walls, except at the face of the entrance (the walls are not shown in the figure for clarity). Other data are as follows:

- Coefficients of static and dynamic friction (for both particles and grains): $\mu_S = \mu_D = 0$
- Rolling resistance coefficient (for both particles and grains): $\mu_R = 0$
- Contact normal damping ratio (for particle-particle, particle-grain, and particle-wall contacts): $\xi_n = 0.1$
- Fluid velocity field: $\mathbf{v}_f = at\mathbf{n}_f$ (outside the specimen) and $\mathbf{v}_f = 0$ (inside the specimen)
- Pressure gradient inside the specimen: $\nabla p = 0.001, 0.002, 0.005, 0.01, \text{ and } 0.02$ kPa/m
- Time at the end of a simulation: $t_{final} = 50$ s
- Time-step size: $\Delta t = 1 \times 10^{-4}$ s, with explicit time integration

The piston is sensible to contact forces from the particles, implying that it may decelerate if these contacts are significant, occasionally receding backward if they overcome the piston's driving acceleration. Figure 3 shows snapshots of the system's configuration at selected time instants, as obtained with our simulation for the case with $\nabla p = 0.01$ kPa/m. As can be seen, in the initial stages the particles of the fluid enter the solid without much difficulty, leading to a quite significant initial flow rate. At some point, though, due to successive collisions with the grains at the entrance of the solid, they start to accumulate in the inlet, which in turn decelerates the piston. After some time, equilibrium between the particles and piston is attained, and the system reaches a more or less steady-state condition, with the flow through the solid evolving at a nearly constant rate (apart from small perturbations at the entrance).

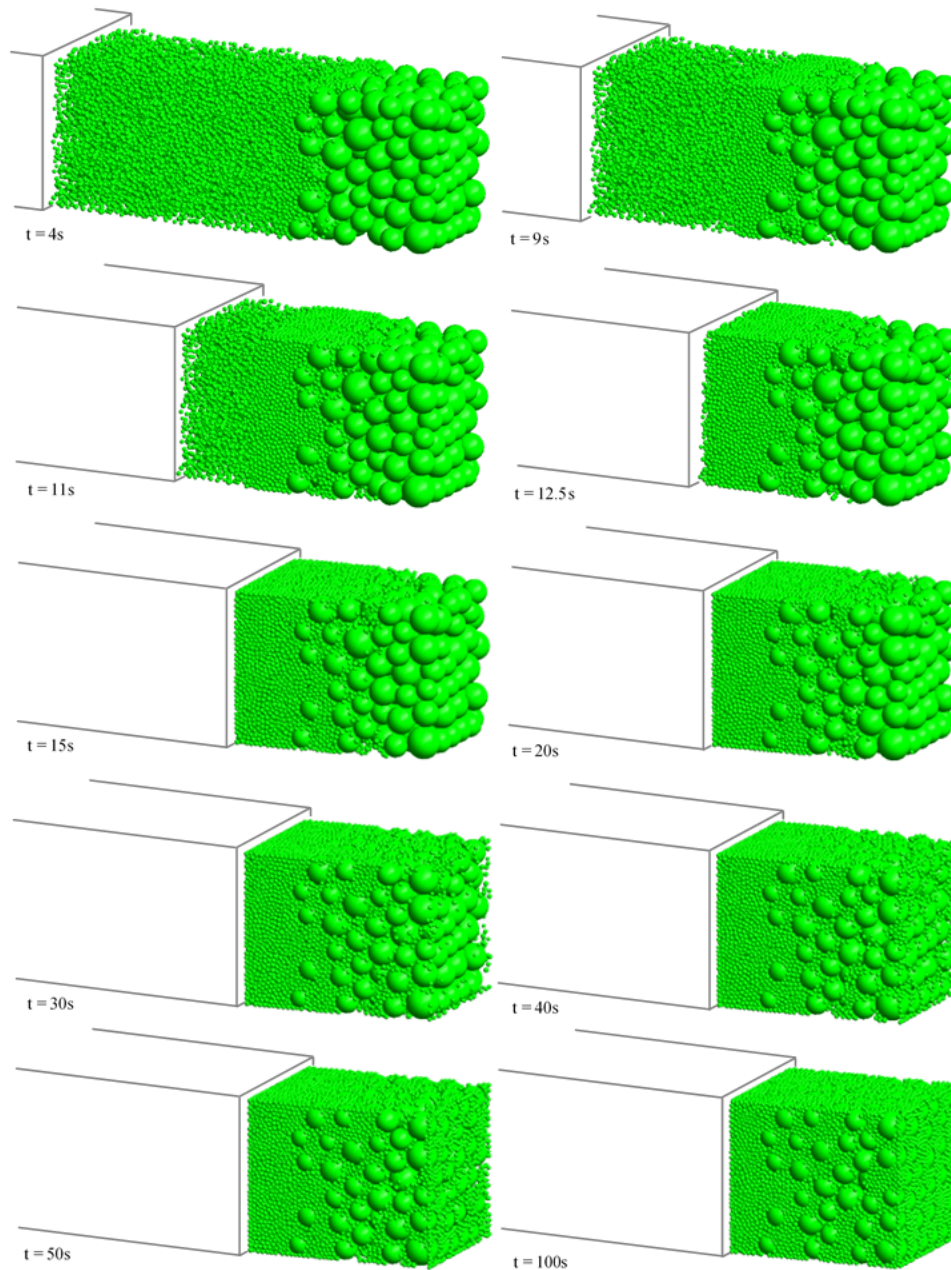


FIG. 3: Snapshots of the system's configuration at selected time instants for $\nabla p = 0.01$ kPa/m. Sequence is from left to right, top to bottom.

This behavior is captured in the graph presented in Fig. 4, wherein the time evolution of the accumulated volume of particles that have traversed a certain cross section of the specimen is shown for two different cross sections (one at the entrance, the other at the mid-length).

Accordingly, at around $t \approx 10$ s, the steady-state phase is reached and the flow progresses at a virtually constant rate for both sections. The accumulated volume predicted by Eq. (16) for the entrance section is also plotted for comparison. As can be seen, the three curves are almost exactly parallel in the steady-state phase, indicating an excellent

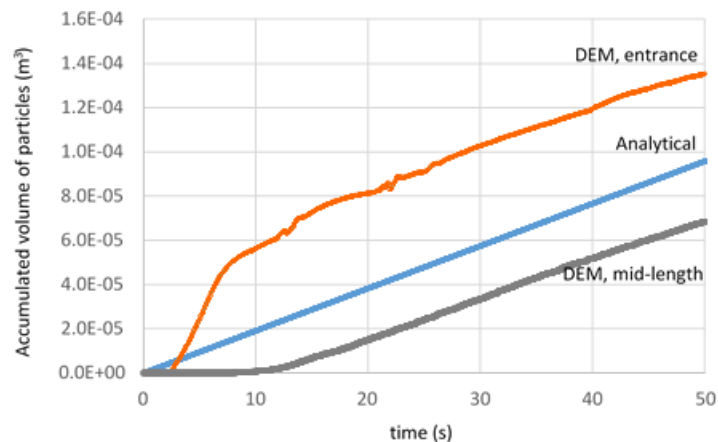


FIG. 4: Time history of the accumulated volume of particles that have traversed the entrance and the mid-length cross sections of the specimen for $\nabla p = 0.01$ kPa/m. The analytical results refer to the entrance section and are computed by multiplying the volume of infiltrated fluid (as predicted by the analytical model) by the particle's volume fraction $v_p = 0.15$.

agreement between the analytical and numerical volumetric flow rates. The exact numbers obtained are $Q_{anal} = 1.92 \times 10^{-6}$ m³/s (analytical), $Q_{DEM,entr} = 1.97 \times 10^{-6}$ m³/s (DEM at entrance section), and $Q_{DEM,mid} = 1.86 \times 10^{-6}$ m³/s (DEM at mid-length section). Another important result is the average velocity of the particles within the specimen at the steady-state phase, which may be estimated by $v = q/v_2$, i.e., by the ratio of the fluid's volumetric flow rate per unit area to the volume fraction of "voids" in the granular solid. From the analytical model, it follows that $v = 2.84 \times 10^{-3}$ m/s; whereas from the DEM simulation, we obtain $v \in [2.71 \times 10^{-3}, 2.96 \times 10^{-3}]$ m/s in the steady-state phase (results vary according to the time instant); this is computed by taking the average of the velocities of only the flowing particles within the specimen at a given time instant of the steady-state phase. This indicates a good agreement also in terms of velocities. Results for the other values of ∇p are shown in Fig. 5 and Table 1. Very good agreement is found between the analytical model and the DEM simulations for all pressure gradients, except for $\nabla p = 0.02$ kPa/m. At this pressure level, the Reynolds number of the flow starts to exceed the maximum value possible for Darcy-like (slow) viscous flows, which is around $Re \approx 10$, and thereby the analytical results are no longer reliable.

One may quickly assess what happens to the infiltration if some of the process parameters are changed. If, for example, the particles have nonsmooth surfaces with nonzero friction coefficients, the volumetric flow rates may change dramatically. This can be seen in Fig. 6, wherein time histories of the infiltrated volume of particles are shown as computed for three different values of $\mu_S = \mu_D$ (0.1, 0.2, and 0.5) at a fixed pressure gradient $\nabla p = 0.01$ kPa/m (and yet, with a very small rolling resistance coefficient $\mu_R = 0.05$). One can see that the infiltration may be severely affected, even to the point of a complete obstruction of the specimen's entrance cross section.

The computation time required for a typical simulation in this model problem is ~ 0.06 h/1.0 s of the problem's duration in a standard, single-processor laptop computer at 2.0 GHz with no parallelization or usage of a graphics-processing unit to leverage performance. We recall that we adopted $\Delta t = 1 \times 10^{-4}$ s in all simulations. The total number of particles is $N_{P,fluid} = 21,500$ for the fluid particles and $N_{P,solid} = 215$ for the porous solid.

7. SUMMARY AND CONCLUSIONS

Particle-laden fluids are widespread in a number of technological applications. Because the presence of particles increases the overall viscosity of the fluid, the pressure gradients needed to pump such fluids through (porous) solid materials can increase dramatically. The present model and computational framework can provide a useful tool for designing systems that pump particle-laden fluids, with the purpose to be able to infiltrate porous materials and deliver desired particles to functionalize the overall material.

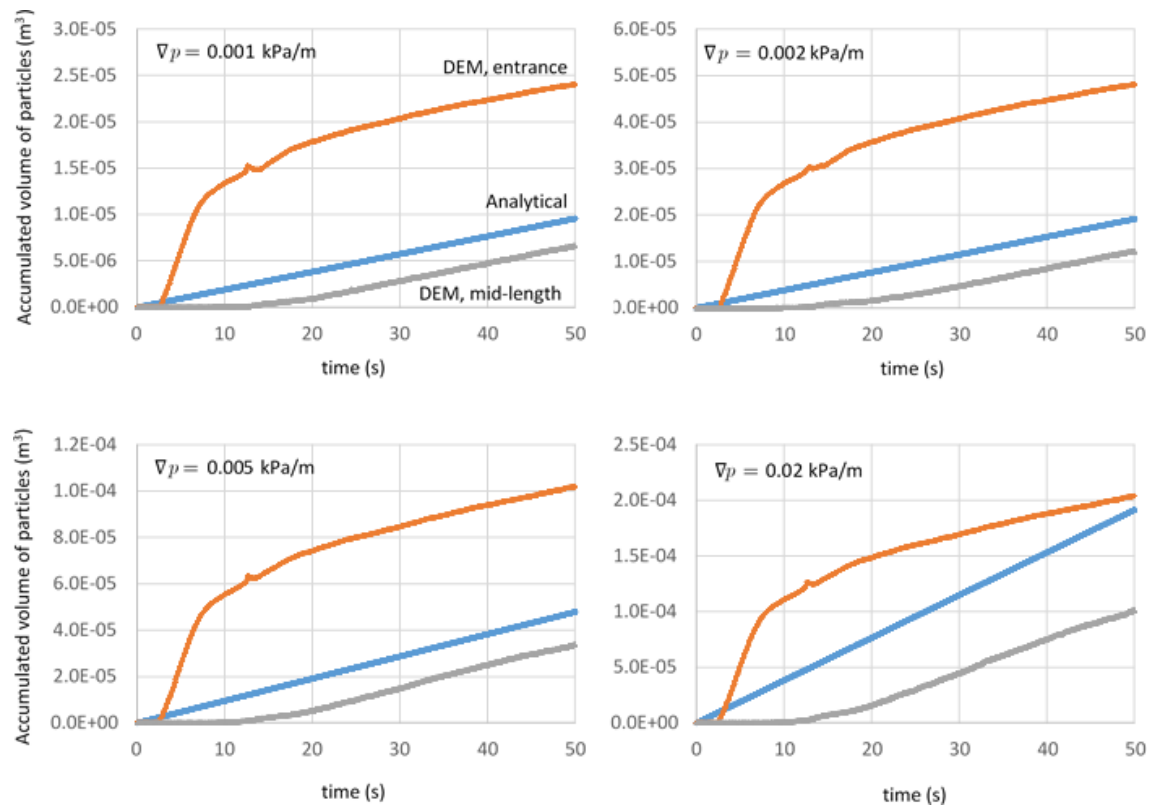


FIG. 5: Time histories of the accumulated volume of particles that have traversed the entrance and the mid-length cross sections of the specimen for all values of ∇p . The analytical results refer to the entrance section and are computed by multiplying the volume of infiltrated fluid (as predicted by the analytical model) by the particle's volume fraction $v_p = 0.15$. Note that the vertical scales of the graphs are not the same.

TABLE 1: Results for different values of the pressure gradient: particle volumetric flow rates (measured in cubic meters per second) and particle average velocity inside the specimen at the steady-state phase (measured in meters per second)

Pressure gradient (m ³ /s)	Q (analytical)	Q (DEM, entrance)	Q (DEM, mid-length)	Velocity (analytical)	Average velocity (DEM)
0.001	1.92×10^{-7}	1.95×10^{-6}	1.93×10^{-6}	2.84×10^{-4}	$2.69 \times 10^{-4} \sim 2.94 \times 10^{-4}$
0.002	3.84×10^{-7}	4.09×10^{-7}	3.72×10^{-7}	5.68×10^{-4}	$5.12 \times 10^{-4} \sim 5.87 \times 10^{-4}$
0.005	9.62×10^{-7}	9.68×10^{-7}	9.71×10^{-7}	1.42×10^{-3}	$1.01 \times 10^{-3} \sim 1.76 \times 10^{-3}$
0.01	1.92×10^{-6}	1.97×10^{-6}	1.86×10^{-6}	2.84×10^{-3}	$2.71 \times 10^{-3} \sim 2.96 \times 10^{-3}$
0.02	3.84×10^{-6}	2.24×10^{-6}	2.65×10^{-6}	5.68×10^{-3}	$4.13 \times 10^{-3} \sim 4.96 \times 10^{-3}$

This paper derived an expression for the pressure gradient needed to attain a given flow rate within a porous medium as a function of four important governing parameters of the infiltration process. We believe it is easy to use by engineers, analysts, and researchers in the field for quick calculations and rapid daily simulations. In particular, the present analysis and numerical model can provide a useful guide to designing and interpreting experiments. However, although the model can provide qualitative information on the infiltration process as a whole, extensions (if intended to capture localized effects, especially those stemming from the fluid flow) are almost certainly going to require complex spatial-temporal discretizations in order to resolve the multiparticle, particle-fluid interactions.

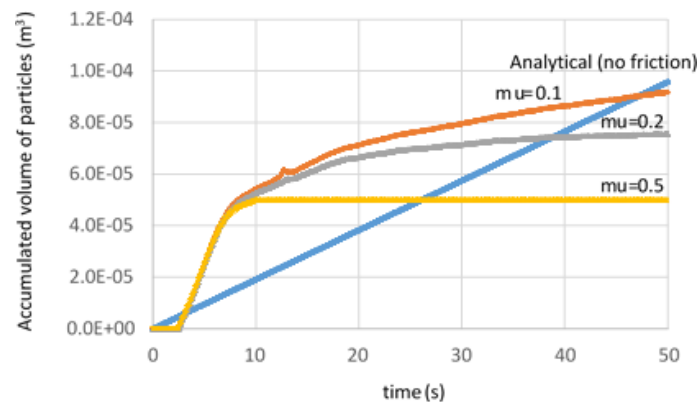


FIG. 6: Analyses results for nonsmooth particles. Time histories of the accumulated volume of particles that have traversed the entrance cross section of the specimen for friction coefficients of 0.1, 0.2, and 0.5, at fixed $\nabla p = 0.01$ kPa/m. The analytical curve (no friction) is also displayed for reference.

Such particle/fluid systems are strongly coupled, due to the drag forces induced by the fluid onto the particles and vice-versa. For example, in Zohdi (2007, 2014), a flexible and robust solution strategy was developed to resolve coupled systems comprised of large groups of flowing particles embedded within a continuous flowing fluid. The focus of that work was to develop adaptive time-stepping schemes, which properly resolve the coupling, via a staggered recursive time-stepping process. The approach can be used in conjunction with computational fluid mechanics codes based on finite difference, finite element, finite volume, or discrete element discretizations, for example, such as those developed in Oñate et al. (2008, 2011, 2014), Rojek et al. (2012), Carbonell et al. (2010), Leonardi et al. (2014), Cante et al. (2014), Bolintineanu et al. (2014), and Avci and Wriggers (2012).

We mention that oftentimes the detrimental growth of channel walls (thus clogging feed lines) starts with the adhesion of particles to the channel's surfaces. This is a complex process, which is likely to involve low fluid-induced shear stress (allowing particles to stick to the walls [see, Zohi (2005, 2014) and Zohdi et al. (2002)], the consideration particle-structure interaction [see, e.g., Neto and Campello (2017)] and strongly coupled diffusive, chemical effects as well as thermal effects. The application of such computational procedures to the problems considered in this paper is under current investigation by the authors. Finally, we mention that other properties of heterogeneous materials, although not needed in the analyses shown here, may be computed through the very same approach proposed in this work. For example, from an electromagnetic standpoint, one may wish to functionalize the porous material in a way as to enhance its overall electrical permittivity or magnetic permeability, from electromagnetically active particles. The estimates for these effective properties are identical in form to the estimates of the effective viscosity and effective permeability shown here.

ACKNOWLEDGMENTS

The second author acknowledges the support from CNPq (Conselho Nacional de Desenvolvimento Científico e Tecnológico) and FAPESP (São Paulo State Science Foundation), under Grants Nos. 309748/2015-1, 307368/2018-1, and 2012/04009-0.

REFERENCES

- Avci, B. and Wriggers, P., A DEM-FEM Coupling Approach for the Direct Numerical Simulation of 3D Particulate Flows, *J. Appl. Mech.*, vol. 79, p. 010901, 2012.
- Biringen, S. and Chow, C.-Y., *An Introduction to Computational Fluid Mechanics by Example*, Hoboken, NJ: Wiley, 2011.
- Bolintineanu, D.S., Grest, G.S., Lechman, J.B., Pierce, F., Plimpton, S.J., and Schunk, P.R., Particle Dynamics Modeling Methods for Colloid Suspensions, *Comput. Particle Mech.*, vol. 1, no. 3, pp. 321–356, 2014.

- Campello, E.M.B., A Description of Rotations for DEM Models of Particle Systems, *Comput. Particle Mech.*, vol. **2**, pp. 109–125, 2015a.
- Campello, E.M.B., Computational Modeling and Simulation of Rupture of Membranes and Thin Films, *J. Brazil. Soc. Mech. Sci. Eng.*, vol. **37**, pp. 1793–1809, 2015b.
- Campello, E.M.B., A Computational Model for the Simulation of Dry Granular Materials, *Int. J. Nonlinear Mech.*, vol. **106**, pp. 89–107, 2018.
- Campello, E.M.B. and Cassares, K.R., Rapid Generation of Particle Packs at High Packing Ratios for DEM Simulations of Granular Compacts, *Latin Am. J. Solids Struct.*, vol. **13**, pp. 23–50, 2016.
- Campello, E.M.B. and Zohdi, T., A Computational Framework for Simulation of the Delivery of Substances into Cells, *Int. J. Numer. Methods Biomed. Eng.*, vol. **30**, pp. 1132–1152, 2014a.
- Campello, E.M.B. and Zohdi, T., Design Evaluation of a Particle Bombardment System Used to Deliver Substances into Cells, *Comp. Model. Eng. Sci.*, vol. **98**, no. 2, pp. 221–245, 2014b.
- Cante, J., Davalos, C., Hernandez, J.A., Oliver, J., Jonsen, P., Gustafsson, F., and Haggblad, H.A., PFEM-Based Modeling of Industrial Granular Flows, *Comput. Particle Mech.*, vol. **1**, no. 1, pp. 47–70, 2014.
- Carbonell, J.M., Oñate, E., and Suarez, B., Modeling of Ground Excavation with the Particle Finite Element Method, *J. Eng. Mech. (ASCE)*, vol. **136**, pp. 455–463, 2010.
- Einstein, A., A New Determination of Molecular Dimensions, *Ann. Phys.*, vol. **19**, no. 4, p. 289306, 1906.
- Hashin, Z., Analysis of Composite Materials: A Survey, *ASME J. Appl. Mech.*, vol. **50**, pp. 481–505, 1983.
- Hashin, Z. and Shtrikman, S., On Some Variational Principles in Anisotropic and Nonhomogeneous Elasticity, *J. Mech. Phys. Solids*, vol. **10**, pp. 335–342, 1962.
- Hashin, Z. and Shtrikman, S., A Variational Approach to the Theory of the Elastic Behaviour of Multiphase Materials, *J. Mech. Phys. Solids*, vol. **11**, pp. 127–140, 1963.
- Jikov, V.V., Kozlov, S.M., and Olenik, O.A., *Homogenization of Differential Operators and Integral Functionals*, Berlin: Springer-Verlag, 1994.
- Rojek, J., Labra, C., Su, O., and Oñate, E., Comparative Study of Different Discrete Element Models and Evaluation of Equivalent Micromechanical Parameters, *Int. J. Solids Struct.*, vol. **49**, pp. 1497–1517, 2012.
- Johnson, K.L., *Contact Mechanics*, Cambridge: Cambridge University Press, 1985.
- Leonardi, A., Wittel, F.K., Mendoza, M., and Herrmann, H.J., Coupled DEM-LBM Method for the Free-Surface Simulation of Heterogeneous Suspensions, *Comput. Particle Mech.*, vol. **1**, no. 1, pp. 3–13, 2014.
- Markov, K.Z., Elementary Micromechanics of Heterogeneous Media, in *Heterogeneous Media: Micromechanics Modeling Methods and Simulations*, K.Z. Markov and L. Preziosi, Eds., Boston: Birkhauser, pp. 1–162, 2000.
- Mura, T., *Micromechanics of Defects in Solids*, Dordrecht, the Netherlands: Kluwer Academic Publishers, 1993.
- Muskat, M., *The Flow of Homogeneous Fluids through Porous Media*, New York: McGraw-Hill, 1937.
- Muskat, M. and Meres, M.W., The Flow of Heterogeneous Fluids through Porous Media. *J. Appl. Phys.*, vol. **7**, pp. 346–363, 1936.
- Neto, A.G. and Campello, E.M.B., Granular Materials Interacting with Thin Flexible Rods, *Comput. Particle Mech.*, vol. **4**, no. 2, pp. 229–247, 2017.
- Oñate, E., Celiueta, M.A., Idelsohn, S.R., Salazar, F., and Surez, B., Possibilities of the Particle Finite Element Method for Fluid-Soil-Structure Interaction Problems, *Comput. Mech.*, vol. **48**, pp. 307–318, 2011.
- Oñate, E., Celiueta, M.A., Latorre, S., Casas, G., Rossi, R., and Rojek, J., Lagrangian Analysis of Multiscale Particulate Flows with the Particle Finite Element Method, *Comput. Particle Mech.*, vol. **1**, no. 1, pp. 85–102, 2014.
- Oñate, E., Idelsohn, S.R., Celiueta, M.A., and Rossi, R., Advances in the Particle-Finite Element Method for the Analysis of Fluid-Multibody Interaction and Bed Erosion in Free Surface Flows, *Comput. Methods Appl. Mech. Eng.*, vol. **197**, nos. 19–20, pp. 1777–1800, 2008.
- Torquato, S., *Random Heterogeneous Materials: Microstructure and Macroscopic Properties*, New York: Springer-Verlag, 2002.
- Zohdi, T.I., *Dynamics of Charged Particulate Systems: Modeling, Theory and Computation*, New York: Springer, 2012.
- Zohdi, T.I., Computation of Strongly Coupled Multifield Interaction in Particle-Fluid Systems, *Comput. Methods Appl. Mech. Eng.*, vol. **196**, pp. 3927–3950, 2007.

- Zohdi, T.I., Embedded Electromagnetically Sensitive Particle Motion in Functionalized Fluids, *Comput. Particle Mech.*, vol. **1**, pp. 27–45, 2014.
- Zohdi, T.I., Monteiro, P.J.M., and Lamour, V., Extraction of Elastic Moduli from Granular Compacts, *Int. J. Fracture/Lett. Micromech.*, vol. **115**, pp. L49–L54, 2002.